Volume 149
Number 22
21 November 2024
Pages 5363-5574

Analyst

rsc.li/analyst

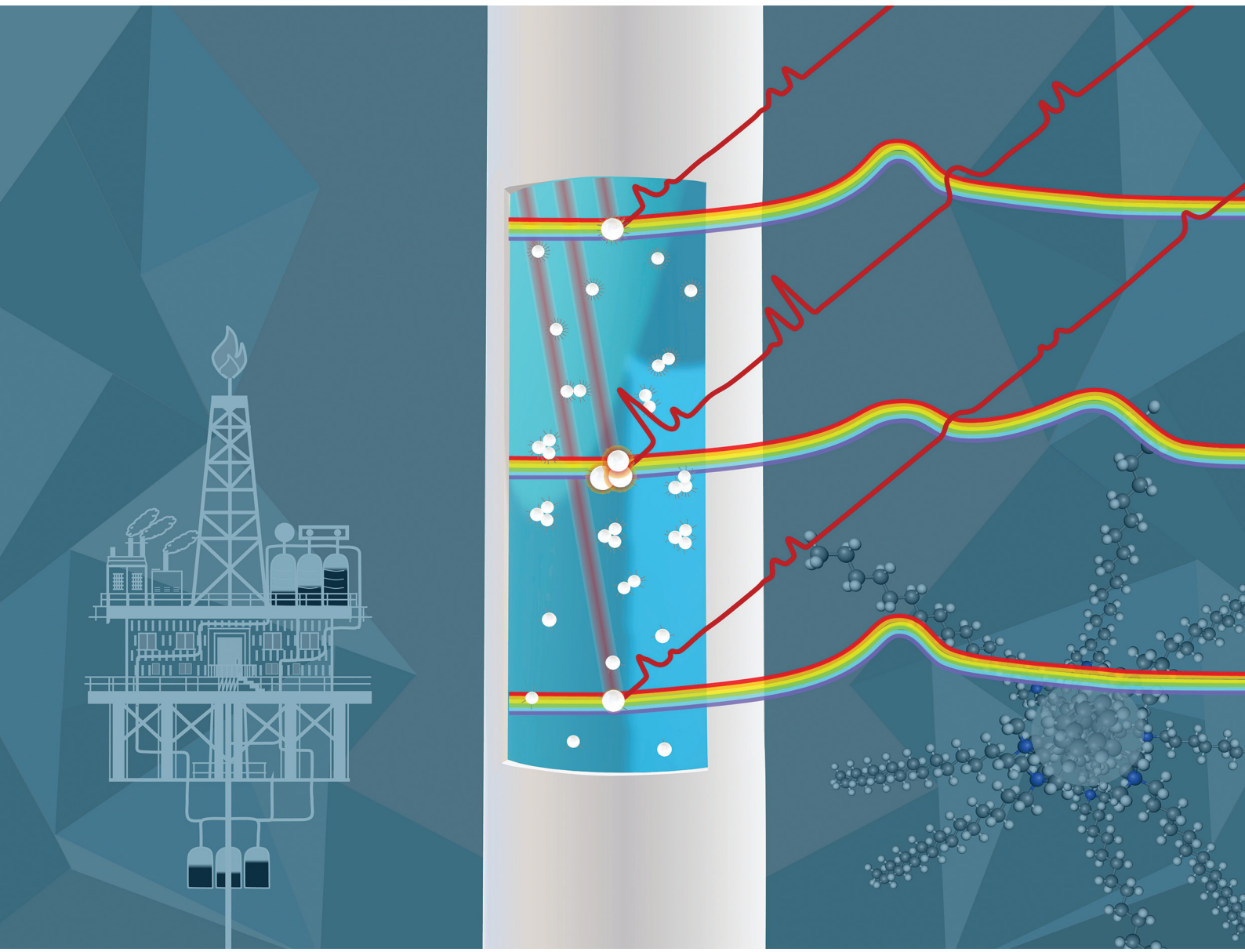

ISSN 0003-2654

ROYAL SOCIETY OF CHEMISTRY

PAPER

Felix Frank, Bernhard Lendl *et al.*
In situ study of the interactions between metal surfaces and cationic surfactant corrosion inhibitors by surface-enhanced Raman spectroscopy coupled with visible spectroscopy

Analyst

PAPER

View Article Online
View Journal | View Issue

Cite this: *Analyst*, 2024, **149**, 5372

In situ study of the interactions between metal surfaces and cationic surfactant corrosion inhibitors by surface-enhanced Raman spectroscopy coupled with visible spectroscopy†

Felix Frank, [a] Daniela Tomasetig, [a] Peter Nahringbauer,[a] Wolfgang Ipsmiller, [b] Gerd Mauschitz,[b] Karin Wieland [c] and Bernhard Lendl *[a]

Cationic surfactants are widely used as corrosion inhibitors for industrial tubings and pipelines. They protect the surface of steel pipes through a film-forming mechanism, providing both anodic and cathodic inhibition. To improve the efficiency of the corrosion protection, it is essential to understand the interactions between the surfactants and metal surfaces. To achieve this, surface enhanced Raman spectroscopy (SERS) can serve as a powerful tool due to its surface sensitivity and potential to detect trace amounts of analytes in complex media. In this contribution, we have investigated the behaviour of *in situ* prepared AgNPs in the presence of benzalkonium chloride as a model corrosion inhibitor using SERS coupled to visible spectroscopy and combined with light scattering methods. By combining these experimental methods, we were able to correlate the aggregation of silver particles with the concentration of added surfactant in the resulting mixture. Using this insight, we also established a SERS method for the detection of benzalkonium chloride traces in water. For this, we utilised the quenching of the SERS response of methylene blue by competitive adsorption of methylene blue and the surfactant on SERS active AgNPs. We believe that our approach can serve a variety of applications to improve the industrial water treatment. For example, the modelling of the interaction of different surfactants with SERS can be used for process intensification, and ultimately, to move towards the digital twinning of corrosion processes for more efficient corrosion inhibition. Furthermore, the ability to adapt our sensing protocol for on-line corrosion inhibitor monitoring allows a fast response to process changes, hence, enabling resource-efficient, continuous process control.

Received 17th June 2024,
Accepted 24th August 2024

DOI: 10.1039/d4an00861h

rsc.li/analyst

1 Introduction

In water treatment for large industrial plants, corrosion of pipelines is one of the most important cost factors, as excessive corrosion leads to shorter maintenance intervals and, thus, increased costs. A prominent method for the surface protection of steel materials in pipelines is the application of corrosion inhibitors whose working principle is based on a film forming mechanism. Inhibitors showing this behaviour include various organic compounds such as acetylenic alcohols, aromatic aldehydes and various nitrogen-containing heterocyclic compounds, as well as long-chain quaternary ammonium compounds (quats). The films formed by these compounds can inhibit both anodic dissolution of pipeline metal and cathodic hydrogen evolution.[1,2] However, their efficiency and inhibition potential can vary greatly with changing operating conditions, which can increase the likelihood of corrosion-related failures and unscheduled downtime.[3] With respect to quats, their interactions with the metal surface have been extensively studied, while the exact mechanisms responsible for corrosion inhibition are still not fully understood.[4,5] As a result, many industrial facilities rely on formulations that have previously shown successful results, rather than actively dosing to respond to changes in the process. This leads to two important research problems. On the one hand, it is essential to learn more about the interactions at the metal-water interface in order to accurately model these processes forming the foundation of moving toward digital twinning of pipelines for corrosion protection purposes, which has the

[a]*Institute of Chemical Technologies and Analytics, TU Wien, Getreidemarkt 9, 1060 Wien, Austria. E-mail: bernhard.lendl@tuwien.ac.at*
[b]*Institute of Chemical, Environmental and Bioscience Engineering, TU Wien, Getreidemarkt 9, 1060 Wien, Austria*
[c]*Competence Center CHASE GmbH, Ghegastrasse 3, 1030 Wien, Austria*

†Electronic supplementary information (ESI) available: Additional explanation of the experimental parameters and considerations for the comparison of different volumetric ratios. See DOI: https://doi.org/10.1039/d4an00861h

potential to actively respond to process changes in real time and provide optimal inhibition performance.[6] On the other hand, until a more efficient method of corrosion inhibitor formulation is established, it is necessary to accurately monitor corrosion inhibitor levels as frequently as possible or financially feasible. By doing this, a consistent dosage and effective treatments can be maintained. Traditionally, inhibitors are measured by taking water samples and measuring them offline with time-consuming, labor- and resource-intensive colorimetric assays or by titration. With both approaches, a two-phase titration[7] based on the method proposed by Epton[8] as well as the colorimetric approach,[9] inhibitor concentrations in the mg L^{-1}-range can be detected, with measurement times depending on the sample and the trained operator. Raman spectroscopy is a non-destructive and molecule specific method that can accurately measure water samples, as water is a weak Raman scatterer. This results in low interferences of water with the Raman spectrum, making the technique an excellent candidate for the monitoring of aqueous process streams.[10,11] However, the inelastically scattered light representing the spontaneous Raman spectrum is weak, resulting in generally low sensitivities.[12] Therefore, it is often not applicable for monitoring process chemicals that are present at trace levels, such as corrosion inhibitors. Surface-enhanced Raman spectroscopy (SERS) is a powerful technique that enhances the inherently weak Raman signal by several orders of magnitude using metallic nanostructures in close proximity to the target analyte.[13] The enhancement is attributed to the localised surface plasmon resonance (LSPR) of the metal, which results in an enhanced electromagnetic field near the surface that enhances both incident and scattered light.[14] SERS is widely used for the detection of various analytes such as drugs, pesticides or explosives at low concentrations with a wide range of applications ranging from biomedical sensing to environmental monitoring, food safety, materials or forensic science.[15–19] In addition to the greatly enhanced sensitivity, the advantages of SERS include ease of sample preparation and speed of analysis.[20] On the other hand, some of the disadvantages of SERS include reproducibility and applicability in real-life scenarios.[21,22]

Moreover, the surface sensitivity of SERS enables detailed analysis of adsorption processes and surface reactions.[23] This was exploited in this study investigating the interaction of quats with AgNPs, using their similar negative surface (zeta) potentials compared to stainless steel[24] to simulate the film forming mechanism[25] on the nanoscale. The postulation that the interaction between the surfactants and the silver and stainless steel surfaces, respectively, can be compared, is based on the assumption that no chemical reaction happens between the surfactants and the respective surfaces and the attraction is purely of electrostatic and hydrophobic nature. We studied their aggregation at different quat concentrations using an excitation laser centered on the shifted extinction band observed for aggregated particles (785 nm, hypothesis of interactions shown in Fig. 1). This allowed us to obtain a SERS signal dependent on the aggregation-induced shift of the visible (VIS) extinction spectrum. We explored this *in situ* using a custom flow cell that allows both SERS and VIS spectroscopy. These results were then correlated with data obtained on particle aggregate size and zeta potential from dynamic light scattering (DLS) to provide a more comprehensive view of the interactions between the metal surface and the quats. Finally, we used this system to establish a detection protocol for quats in water with good sensitivity in the typical application range of the corrosion inhibitors (10–50 mg L^{-1}). This method makes use of the competitive adsorption of methylene blue (MB) and quats on the AgNPs by looking at the quenching of the MB SERS signal at higher quat concentrations. In conclusion, this work not only provides valuable insight into the processes behind corrosion inhibition moving a step closer to efficient process intensification but also demonstrates the potential of SERS for corrosion inhibitor monitoring in water treatment.

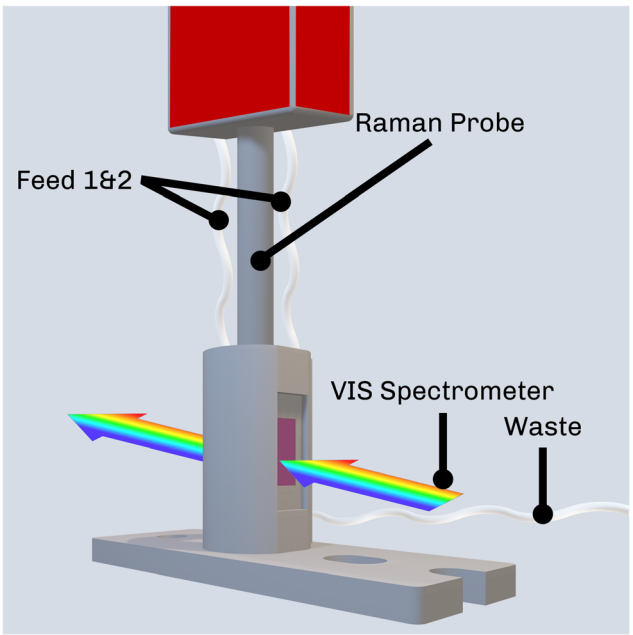

Fig. 1 Hypothesis of the interaction between cationic surfactants and AgNPs. The aggregation of the particles leads to the promotion of hot-spots and a shift in the extinction spectrum towards the Raman laser line, both enhancing the SERS spectrum of the adsorbed surfactant molecules.

2 Materials and methods

2.1 Used reagents

Silver nitrate ($AgNO_3$, Sigma-Aldrich, >99.0%), Hydroxylammonium chloride ($NH_2OH{\cdot}HCl$, Sigma-Aldrich, 99.999%), Sodium hydroxide (NaOH, Sigma-Aldrich, >98% anhydrous), Benzyldimethylhexadecylammonium chloride (BAC-16, Sigma-Aldrich) and Methylene blue (MB, Sigma-Aldrich, p.a.) were used as received, Nitric acid (HNO_3, Sigma-Aldrich, 70%) was diluted to a 2 M solution with deionised water for cleaning purposes.

2.2 Studies of the interaction between AgNPs and BAC-16

For the SERS measurement, a custom-made aluminium flow cell equipped with optical grade windows designed to fit into the sample compartment of a Cary 50 Bio UV-VIS spectrometer (Agilent, USA) with a total usable liquid volume of 12 mL was used. The measurement setup is depicted schematically in Fig. 2. The SERS-active AgNPs were prepared by reducing silver nitrate with hydroxylamine using a modified version of the procedure proposed by Leopold and Lendl.[26] For this, a 1.11 ·M $AgNO_3$ stock solution and solution of the reducing agent containing 15 mM $NH_2OH{\cdot}HCl$ and 30 mM NaOH were prepared. The mechanism of the reaction can be summed up with the following reaction equation:

$$2NH_2OH + 2Ag^+ + 2OH^- \rightarrow 2Ag_{coll}{}^0 + 4H_2O + N_2 \uparrow$$

With the Leopold and Lendl method, monodisperse particles with a median particle radius of 53 nm and an extinction maximum at 430 nm can be synthesised (Fig. 3). Further, no citrate is used for the synthesis of the nanoparticle which could interfere with the BAC-16 bands as would be the case for particles synthesised with the method proposed by Lee and Meisel, as the reaction only produces gaseous side products.[27,28] For the BAC-16 surfactant, a concentration series ranging from 0.02 mg L^{-1} to 100 mg L^{-1} was prepared freshly.

For the study of the interaction between the AgNPs and the surfactants, four measurement series with different AgNP : BAC-16 ratios (1 : 9, 2 : 8, 5 : 5, 8 : 2) were carried out using the mixtures listed in Table 1, with the concentrations referring to the samples before mixing (corrected concentrations after mixing are displayed in Table S2†). Each single measurement was performed according to the following sequence (illustrated in more detail in the Fig. S1†):

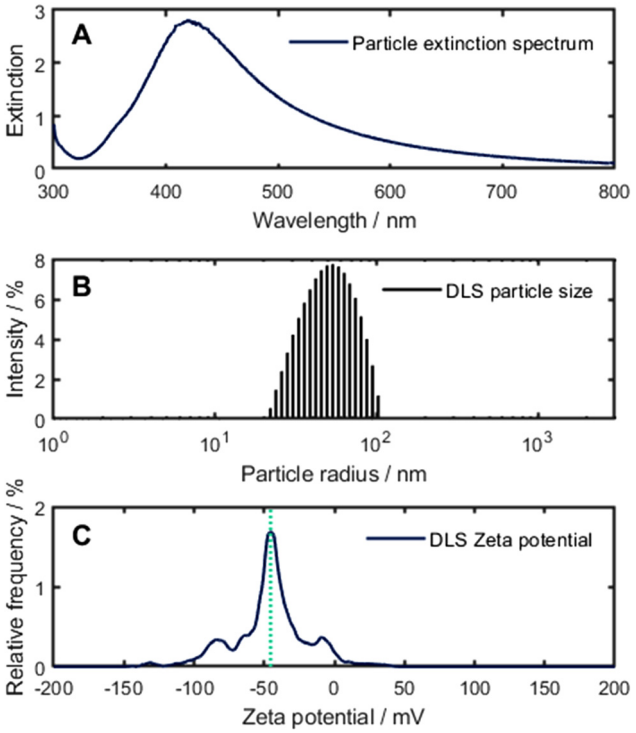

Fig. 3 (A) Extinction spectrum of the pristine AgNPs. (B) DLS particle size distribution for the pristine AgNPs. (C) Zeta potential for the pristine AgNPs, maximum of the potential function (−45 mV) marked with green dotted line.

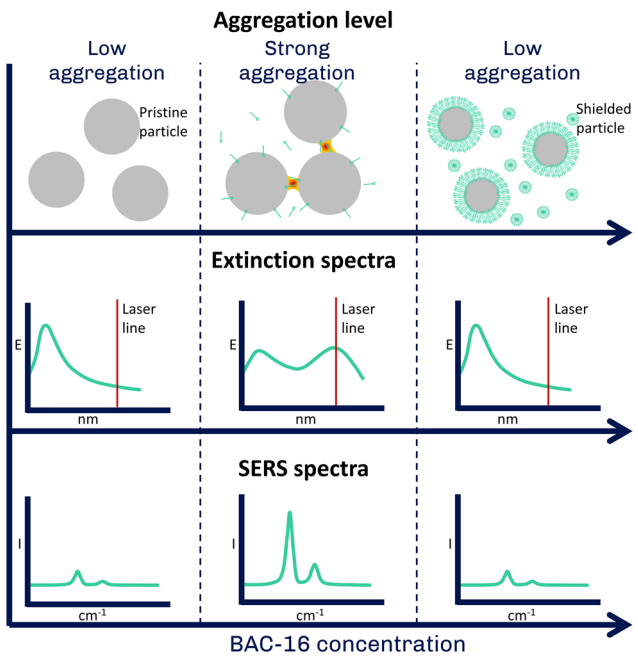

Fig. 2 Schematic depiction of the measurement setup accommodating the Raman probe used for SERS inside the sample compartment of the UV-VIS spectrometer.

First, the stock solutions for the synthesis of the AgNPs were injected into the measurement cell in a 9 : 1 volumetric ratio ($AgNO_3$ to reducing agent) under stirring using a Cimarec i Mini Stirrer (Thermo Fisher Scientific, USA). In order to prevent AgNP formation in the tubings, injection happened using two separate feed lines (Feed 1 & 2 in Fig. 2) for the $AgNO_3$ and the reducing agent, respectively. After 1 min of stirring, the BAC-16 solution was added. 9 min after initial mixing (referring to the addition of BAC-16 to the AgNP colloid), extinction spectra between 350 nm and 800 nm were recorded to ensure the quality of the colloid. Raman measurements were performed 10 min after initial mixing using a WP 785 Raman spectrometer (Wasatch Photonics, USA) with an excitation wavelength of 785 nm fibre-coupled to a WP RP 785 Raman probe (Wasatch Photonics, USA) with an outside diameter of 12.7 mm and a sapphire ball probe tip. The Raman spectra were recorded using the WP Enlighten software, with 10 averages and the exposure time adjusted to prevent detector saturation while maximising the signal. Between individual measurements, the measurement cell, ports, and Raman probe were rinsed with deionised water multiple times until no additional bands compared to the blank were visible in the Raman spectrum. Additionally, the cell was cleaned with a 2 M

Table 1 Experimental parameters for the VIS-SERS measurements. BAC-16 concentrations refer to the samples before mixing

Ratios	V ($AgNo_3$)/mL	V (NH_2OH)/mL	V (BAC-16)/mL	c (BAC-16)/mg L^{-1}								
1 : 9	0.9	0.1	9	0.02	0.05	0.2	0.5	1	2	4		
2 : 8	1.8	0.2	8	0.02	0.05	0.2	0.5	1	2	4		
5 : 5	4.5	0.5	5	0.02	0.05	0.2	0.5	1	2	4	10	100
8 : 2	7.2	0.8	2			0.2	0.5	1	2	4	10	100

HNO_3 solution after each measurement series to avoid the accumulation of Ag on the walls of the flow cell. In order to show the time dependence of the interaction, additional VIS/SERS measurements were performed in 5 min intervals for a total of 45 min.

2.3 Further characterisation of the AgNPs

To give further context on the aggregation of the AgNPs, dynamic light scattering (DLS) was performed on the colloid-surfactant system. For these experiments, the stock solutions for the synthesis of the AgNPs as mentioned above were injected into a glass vial in a 1 : 9 volumetric ratio ($AgNO_3$ to reducing agent) under stirring, resulting in a total of 0.5 mL. After stirring for 90 seconds, 4.5 mL of the surfactant solutions were added and stirred for another eight minutes. Afterwards, 1 mL of the mixture were injected into a polycarbonate cuvette and the DLS measurement started. The DLS measurements were performed on a Litesizer 500 (Anton Paar, Austria) at 25 °C, with temperature stabilisation and calibration of the instrument set at 30 s (total time after particle synthesis was 10 minutes for each measurement). The particle size distribution functions were calculated using ISO 22412[29] and the narrow analysis model in the Kalliope software package (Anton Paar, Austria).

2.4 Trace sensing of BAC-16 using surface-enhanced Raman spectroscopy

For the trace sensing of BAC-16 with SERS, we made use of the competitive adsorption of methylene blue and BAC-16 on the AgNPs. For these measurements, the sequence of the interaction studies was slightly adapted: First, the stock solutions for the synthesis of the AgNPs as mentioned above were injected into the measurement cell in a 1 : 9 volumetric ratio ($AgNO_3$ to reducing agent) under stirring, resulting in a total of 2 mL. This colloidal suspension was then diluted with 7 mL of deionised water. After one minute of stirring, 0.9 mL of the 1 mg L^{-1} MB solution were added. Finally, 0.1 mL of the BAC-16 solution were added after another half a minute. Raman spectra were recorded 10 min after initial mixing of the AgNPs and the MB solution in the same way as for the interaction studies. Between individual measurements, the measurement cell, ports, and Raman probe were rinsed multiple times with deionised water until no additional bands compared to the blank were visible in the Raman spectrum. After each measurement series, the cell was cleaned as mentioned before.

3 Results and discussion

3.1 Evaluation of the surface-enhanced Raman spectra

The pre-treatment of the SERS spectrum involved a baseline correction to remove the fluorescence background. This was done in Matlab R2023b using an adaptation of the iterative algorithm of Lieber and Mahadevan-Jansen (50 iterations, smoothing parameter of the cubic spline set to 0.00001).[30] Afterwards, the bands were referenced to the sapphire band of the Raman probe at 752 cm^{-1} unless stated otherwise. Finally, band heights of the processed Raman spectra were determined and used for data evaluation. Here, we focused on the aromatic C–H in-plane deformation vibration as well as the C–N deformation of the quaternary amine overlapping at 1003 cm^{-1} and the symmetrical C–N vibration at 1390 cm^{-1} for MB.[28,31]

To correlate the experiments with different colloid to surfactant volumetric ratios (Table 1), the concentrations were standardised to reflect the number of BAC-16 molecules per AgNP. For this, two simplifications regarding the particle size were made: First, all particles were assumed to have a particle radius of 53 nm (the median size of the pristine particles) as an average for the unimodal particle size distribution. Additionally, for aggregated silver particles, the surface of the particle aggregates equals the sum of the single particles.

Considering this, the BAC-16 concentrations can be used to estimate the number of BAC-16 molecules per AgNP in suspension to compare the SERS concentration series of different volumetric ratios to each other. The calculation behind this estimation is based on the stoichiometric reduction of the silver with a concentration of 1.11 mmol L^{-1}, which combined with the particle radius and the density and molar mass of silver results in a AgNP concentration (c_{AgNP}) of 1.65×10^{10} particles per mL suspension before mixing with BAC-16 (calculation described in detail in the ESI†). The number of BAC-16 molecules per AgNP (C^*_{BAC}) can then be calculated using the BAC-16 concentration before mixing with the AgNP colloid (c_{BAC}, in mol mL^{-1}) and the volumetric ratio ($x : y$) with the following equation:

$$C^*_{BAC} = \frac{c_{BAC} \cdot N_A \cdot y}{c_{AgNP} \cdot x} \quad (1)$$

3.2 *In situ* study of the interaction between AgNPs and BAC-16

In Fig. 4, the normalised SERS signal (band at 1003 cm^{-1} divided by the highest SERS signal for each measurement

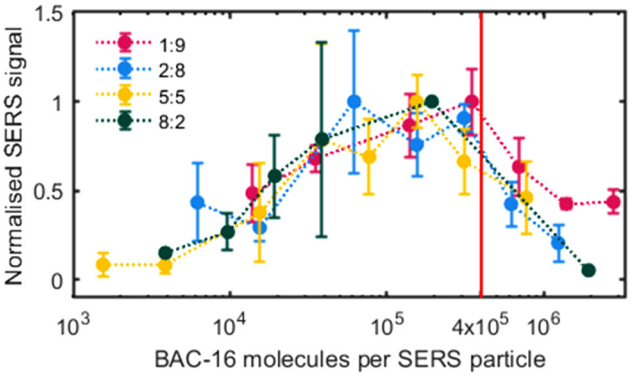

Fig. 4 Normalised SERS signal 10 min after initial mixing for different volumetric ratios (*in situ* synthesised particle/BAC-16 solution) *vs.* BAC-16/particle ratio.

series) for the studied AgNP-BAC-16 surfactant system is shown, which is plotted against the number of BAC-16 molecules per AgNP in suspension (as introduced in the previous section 3.1).

Upon examining the data, it becomes apparent that a positive correlation exists between the SERS response and the BAC-16 concentration when the concentration is below a threshold of about 4×10^5 BAC-16 molecules per AgNP. However, this trend reverses at higher BAC-16 concentrations, resulting in a decrease in the SERS response. This unusual behaviour, where an increase in the analyte concentration results in a decreased SERS response, suggests a change in the surface enhancement on the silver particles. Similar results have been reported by other researchers in this field, correlating the decrease of the SERS response at higher BAC-16 concentrations with the critical micellar concentrations (CMC) of the surfactants.[32] Trying to give a more complete picture of the interactions causing this trend, we focused on studying the aggregation of the AgNPs responsible for the surface enhancement.

For the time dependent extinction spectra (Fig. 5A), a significant shift can be observed between the mixture (2 : 8 AgNP to BAC-16 ratio, 0.5 mg L^{-1} BAC-16) at 0 min (extinction spectrum recorded right after mixing) and 5 min. For these two spectra, the maximum of the second higher wavelength band shifts from 660 nm to around 800 nm. After that, the system stabilises and the extinction decreases over the whole wavelength range. Considering this trend, all SERS experiments were evaluated using the SERS spectrum recorded 10 min after initial mixing.

In Fig. 5B and C, the dependence of the SERS spectra on the BAC-16 concentration is shown for a 2 : 8 AgNP to BAC-16 ratio 10 min after initial mixing. Here, the trend also shown in Fig. 4 can be seen for a single measurement series, with the maximum SERS response being present for a BAC-16 concentration of 0.5 mg L^{-1} (equivalent to 2.5×10^5 BAC-16 molecules per AgNP). Correlating this with the extinction spectra for these respective concentrations in Fig. 5D and E, an interesting

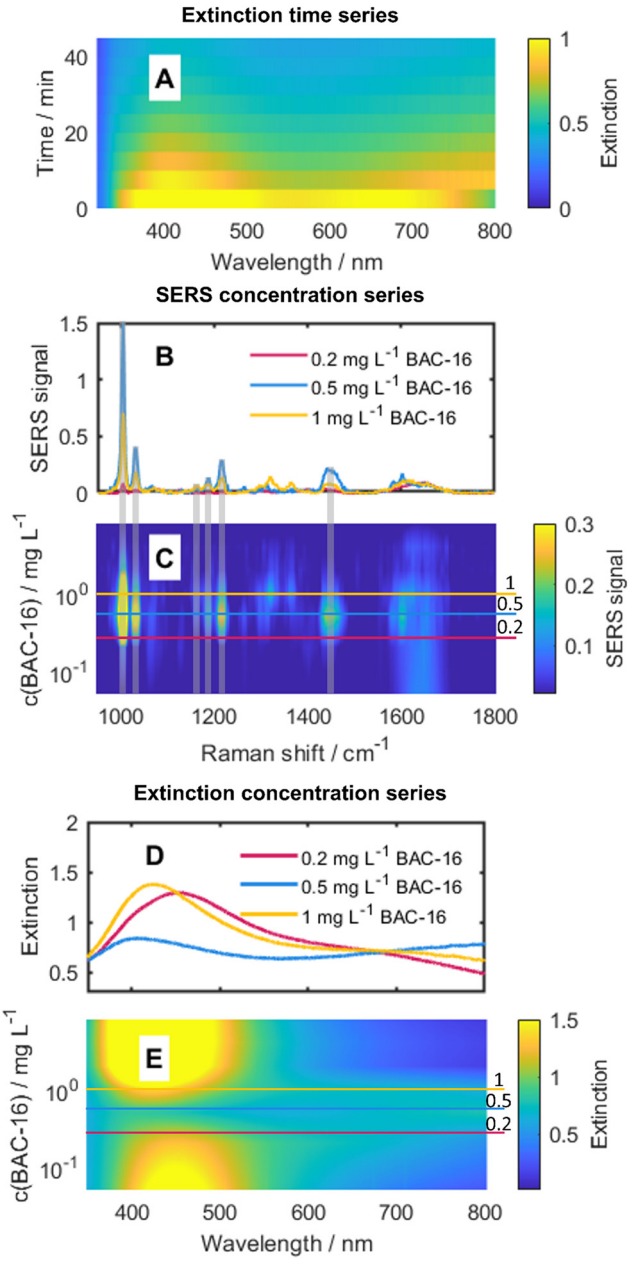

Fig. 5 (A) Time dependence of the extinction spectra of the particles for the interaction with 0.5 mg L^{-1} BAC-16. (B) Exemplary SERS spectra for three different BAC-16 concentrations 10 min after initial mixing. (C) Concentration dependence of the SERS spectra of BAC-16 10 min after initial mixing. (D) Exemplary extinction spectra for three different BAC-16 concentrations 10 min after initial mixing. (E) Concentration dependence of the extinction spectra of the system at different BAC-16 concentrations 10 min after initial mixing. All concentrations refer to a particle/BAC-16 ratio of 2 : 8 (see Table 1).

trend can be found, as the extinction peak broadening primarily happens in the same concentration range in which the highest SERS response can be made out. For all other concentrations, the extinction spectrum closely resembles the spectrum of pristine silver particles (Fig. 3), featuring a single band with a maximum close to 430 nm.

A reason for the broadening of the peaks in the extinction spectra can be found in the aggregation of AgNPs at certain concentrations.[33] As the Stokes (or hydrodynamic) radius of a group of aggregated particles increases, the light scattering behaviour changes. This phenomenon can be explained by the Mie theory, which describes the scattering behaviour of particles with diameters in the same order of magnitude as the wavelength of the incident light.[34] The Mie theory can be used to simulate the theoretical extinction spectra of colloidal metal suspensions or, in turn, estimate the particle size of AgNPs considering their extinction spectra.[35] For the calculations in this work, a Matlab script by Andrea Baldi based on the Mie theory was used.[36] It uses the relative permittivity of a material to compute the extinction cross-section for spherical particles. The permittivity data necessary for these calculations were taken from the work of Johnson and Christy.[37] In Fig. 6, top, the calculated extinction spectra of AgNP with radii between 40 nm and 150 nm are shown, while in Fig. 6, bottom, the simulated extinction spectrum for a colloid with the same particle size distribution as measured for the AgNPs is compared with the measured extinction spectrum. The maxima of both extinction spectra appear at comparable wavelength indicating a consistency between the calculated extinction spectrum of the suspension of the measured particle size distribution with the measured extinction spectrum. The deviation in the shapes of the spectra can be explained by the non-spherical shape of real particles.

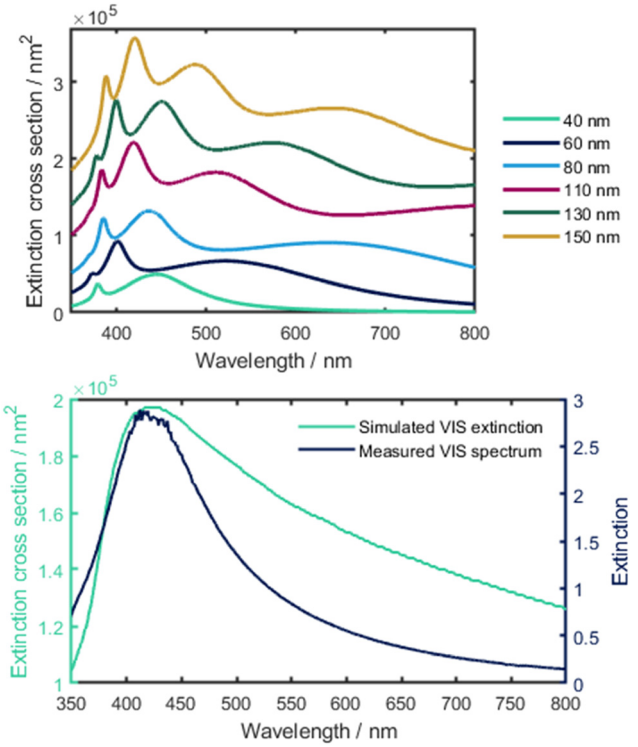

Fig. 6 Top: calculated extinction spectra of different sized AgNPs based on the Mie theory. Bottom: simulated VIS extinction using the particle size distribution *vs.* Measured extinction spectrum.

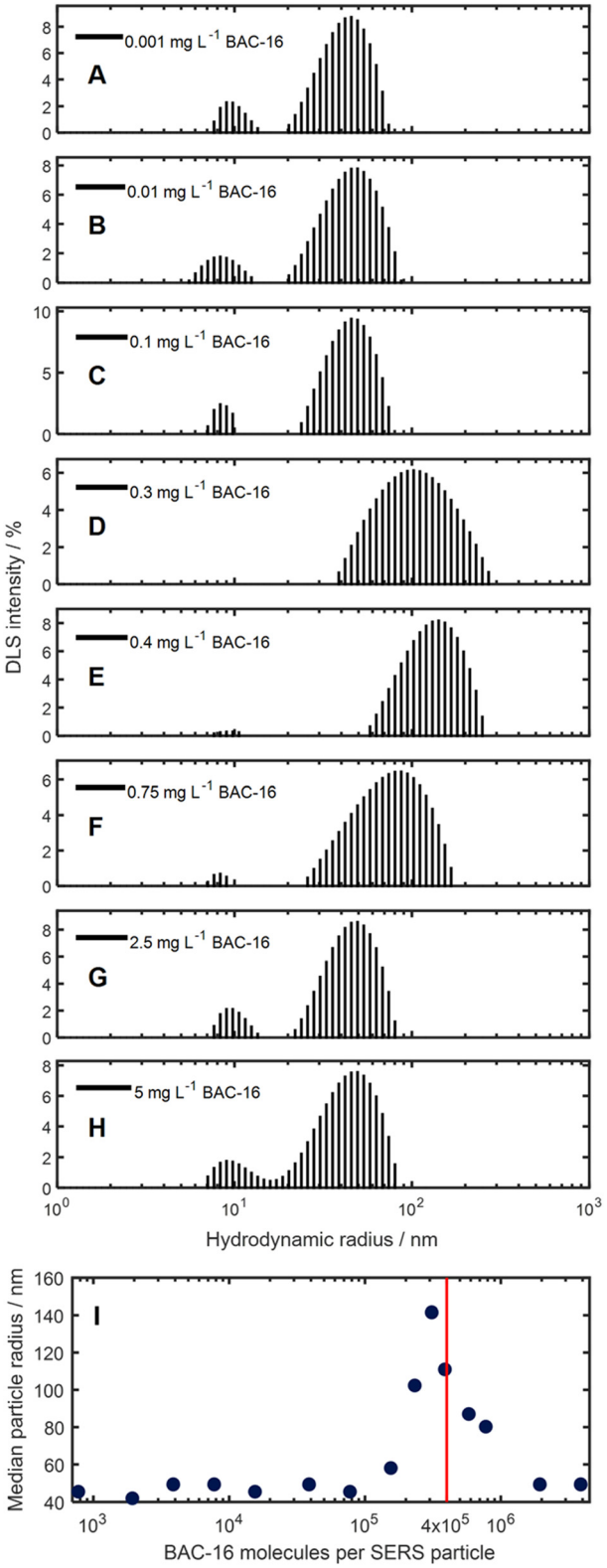

Fig. 7 (A–H) Particle size distributions for freshly synthesised AgNPs mixed with different concentrations of BAC-16 after 10 min. (I) Median particle size for these AgNPs and BAC-16 mixtures, referenced to the BAC-16/particle ratio.

To get actual information on the promotion of particle aggregation at certain BAC-16 concentrations, we investigated their respective particle size distributions obtained through DLS experiment sas a function of BAC-16 concentration. The results of these measurements are shown in Fig. 7. For the AgNP DLS signal, a shift of the median particle radii from 46 nm to 142 nm can be seen for the concentrations between 0.1 and 2.5 mg L^{-1}, with the maximum at a concentration of 0.4 mg L^{-1} (equivalent to a BAC-16/particle ratio of 3.1×10^5). This correlates well with the data gathered from both SERS and VIS, where the threshold, after which the surface enhancement decreases, was determined to be around 4×10^5 BAC-16 molecules per AgNP. The promotion of aggregation determined with DLS can be explained by the formation of micellar encapsulation structures around the AgNPs. A monolayer of BAC-16 increases the van der Waals attraction between encapsulated particles, while for a bilayer, electrostatic repulsion forces lead to a shielding of particles, inhibiting aggregation.

Beside the aggregation-induced shift in the hydrodynamic radius, for some measurements, a small second peak at 10 nm can be detected. This is thought to be an artifact due to the formation of some small BAC-16 covered AgNPs after addition of BAC-16, leading to smaller BAC-16 capped AgNPs.[38,39] However, they can be disregarded for the analysis, as this size region does not contribute significantly to the extinction spectra broadening.

The data from the zeta potential measurements of the particles at higher BAC-16 concentrations could not be translated by the models of the Kalliope software, possibly due to interferences of the BAC-16 micelle formation, while the measurements at lower BAC-16 concentrations led to similar results as obtained for the pristine AgNPs (shown in Fig. 3, bottom).

3.3 Trace sensing of BAC-16 using surface-enhanced Raman spectroscopy

As the direct quantification of BAC-16 is not feasible with the SERS system due to particle shielding at higher surfactant concentrations, a protocol for an indirect measurement of BAC-16 is proposed using a tracer molecule at a constant concentration, whose SERS intensity is reduced upon increasing BAC-16 concentration. For such a tracer, a molecule with a good SERS response and high sensitivity was required. Hence, we chose MB as it fulfils these criteria and its SERS response is well studied.[40] A calibration curve was created to determine the range at which the MB SERS signal shows a steep concentration dependency. The results of these measurements are presented in Fig. 8. When looking at the data, the non-linear nature of the SERS response is observed. As the region of interest was determined in the concentration range below 1 mg L^{-1} (highlighted in red in Fig. 8, bottom), 1 mg L^{-1} MB was chosen for the tracer.

Using the 1 mg L^{-1} MB tracer, a sensing protocol was devised for a concentration range of 10–50 mg L^{-1} BAC-16, which represents typically applied corrosion inhibitor dosages. For other

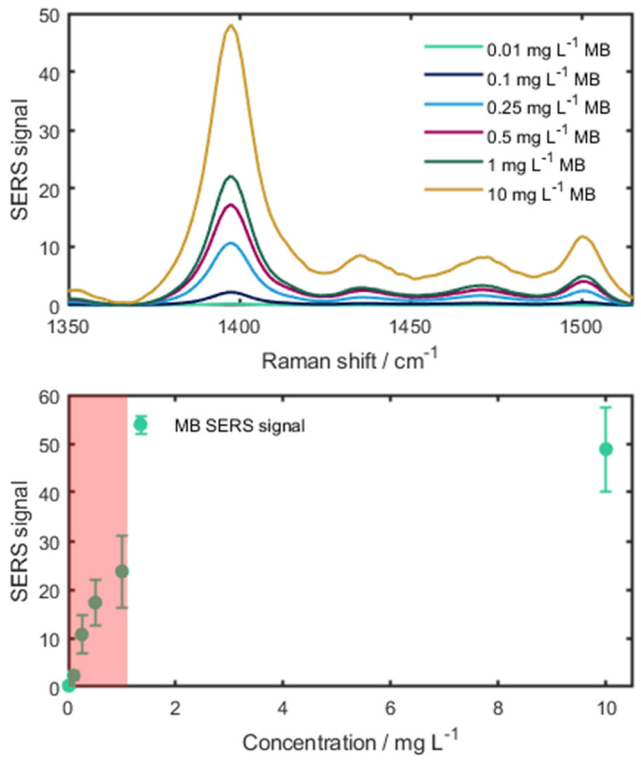

Fig. 8 Top: SERS spectra of different MB concentrations. The pure MB SERS spectra were normalised by the integration time. Bottom: calibration curve of MB showing the region of interest (in red).

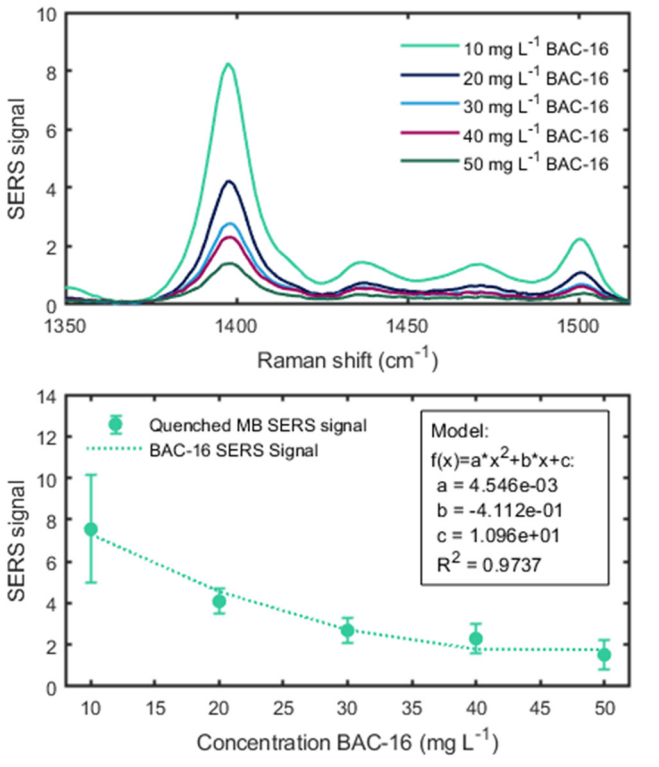

Fig. 9 Top: average (n = 5) SERS spectra of 1 mg L^{-1} MB at different BAC-16 concentrations. Bottom: quenched SERS signal of the MB (n = 5) depending on the BAC-16 concentration for a volumetric ratio of 1 : 0.05 : 0.45 : 3.5 (colloid to BAC-16 to MB to H_2O).

applications, the method can also be scaled by changing the volume ratios of BAC-16 and the deionised water used for dilution. By doing this, the smallest measureable concentration range of this method equates to 150–750 μg L^{-1} BAC-16. The results of the BAC-16 measurements are depicted in Fig. 9, showing a good fit for a second order polynomic function.

4 Conclusion and outlook

In this report, we presented an *in situ* study of the interactions of BAC-16, a representative of cationic surfactants commonly used in corrosion inhibition with metal surfaces. We utilised SERS-active AgNPs as a model system for the protected metal surfaces in the corrosion inhibition process due to similar negative surface potentials. As the aggregation of the AgNPs leads to a broadening of the extinction spectrum and an increase of the surface enhancement, we chose an off-centered laser with an excitation wavelength of 785 nm. We designed and applied a custom flow cell to accommodate both SERS and VIS spectroscopy, showing a maximum of the SERS signal between 1×10^5 and 4×10^5 surfactant molecules per AgNP. We further correlated this with DLS measurements, giving insight into the shielding of the particles by means of their hydrodynamic radius at different surfactant concentrations.

Finally, we used these insights to devise a sensing protocol for BAC-16 in water, utilizing the particle shielding at higher BAC-16 concentrations for the SERS quenching of a MB tracer. With this indirect protocol, we could quantify BAC-16 in the concentration range of 10–50 mg L^{-1}. Upon adapting the mixing ration of the sample and water in the assay, the application range of the calibration function can be shifted, allowing quantification of BAC-16 traces down to 150 μg L^{-1}. This study combines both points of emphasis of corrosion inhibition research with the understanding of the inhibition processes and the quantification of corrosion inhibitors in water samples. We, therefore, believe that this work can serve as a stepping stone for future research in this field with the aim to optimise the use of corrosion inhibitors in industrial processes.

Author contributions

FF: conceptualisation, methodology, investigation, data curation, formal analysis, validation, writing – original draft, visualization. DT: investigation, writing – review & editing. PN: investigation, writing – review & editing. WI: investigation. GM: investigation. KW: methodology, writing – review & editing. BL: conceptualisation, validation, writing – review & editing, funding acquisition, supervision.

Data availability

Data for this article, including the raw data and evaluation scripts are available at Zenodo at **https://doi.org/10.5281/zenodo.11547084**.

Conflicts of interest

There are no conflicts to declare.

Acknowledgements

This work is part of the HYDROPTICS project, which has received funding from the European Union's Horizon 2020 research and innovation program under the grant agreement no. 871529. This project is an initiative of the Photonics Public Private Partnership. His work was further supported by the COMET Centre CHASE, funded within the COMET-Competence Centers for Excellent Technologies Programme by the BMK, the BMDW, and the Federal Provinces of Upper Austria and Vienna. The COMET Programme is managed by the Austrian Research Promotion Agency (FFG).

References

1 N. F. Atta, A. Fekry and H. M. Hassaneen, *Int. J. Hydrogen Energy*, 2011, **36**, 6462–6471.
2 S. M. Wilhelm, *Corrosion*, 1992, **48**, 691–703.
3 M. Schwingenschlögl, PhD thesis, TU Wien, 2023.
4 J. Wang, T. Zhang, X. Zhang, M. Asif, L. Jiang, S. Dong, T. Gu and H. Liu, *J. Mater. Sci. Technol.*, 2020, **43**, 14–20.
5 L. Guo, S. Zhu and S. Zhang, *J. Ind. Eng. Chem.*, 2015, **24**, 174–180.
6 C. D. Taylor, *Corros. Eng., Sci. Technol.*, 2015, **50**, 490–508.
7 V. W. Reid, G. F. Longman and E. Heinerth, *Tenside, Surfactants, Deterg.*, 1968, **5**, 90–96.
8 S. R. Epton, *Nature*, 1947, **160**, 795–796.
9 E. Jurado, M. Fernández-Serrano, J. Núñez-Olea, G. Luzón and M. Lechuga, *Chemosphere*, 2006, **65**, 278–285.
10 K. Wieland, M. Masri, J. von Poschinger, T. Brück and C. Haisch, *RSC Adv.*, 2021, **11**, 28565–28572.
11 D. I. Ellis, R. Eccles, Y. Xu, J. Griffen, H. Muhamadali, P. Matousek, I. Goodall and R. Goodacre, *Sci. Rep.*, 2017, **7**, 12082.
12 E. Smith and G. Dent, *Modern Raman spectroscopy: a practical approach*, John Wiley & Sons, 2019.
13 S. M. Asiala and Z. D. Schultz, *Analyst*, 2011, **136**, 4472–4479.
14 S. Schlücker, *Angew. Chem., Int. Ed.*, 2012, **53**, 4756–4795.
15 J. Fei, L. Wu, Y. Zhang, S. Zong, Z. Wang and Y. Cui, *ACS Sens.*, 2017, **2**, 773–780.
16 J. Ando, M. Asanuma, K. Dodo, H. Yamakoshi, S. Kawata, K. Fujita and M. Sodeoka, *J. Am. Chem. Soc.*, 2016, **138**, 13901–13910.
17 S. Pang, T. Yang and L. He, *TrAC, Trends Anal. Chem.*, 2016, **85**, 73–82.
18 A. Chou, E. Jaatinen, R. Buividas, G. Seniutinas, S. Juodkazis, E. L. Izake and P. M. Fredericks, *Nanoscale*, 2012, **4**, 7419–7424.

19 D. Cialla, A. März, R. Böhme, F. Theil, K. Weber, M. Schmitt and J. Popp, *Anal. Bioanal. Chem.*, 2012, **403**, 27–54.
20 R. Goodacre, D. Graham and K. Faulds, *TrAC, Trends Anal. Chem.*, 2018, **102**, 359–368.
21 R. Shi, X. Liu and Y. Ying, *J. Agric. Food Chem.*, 2018, **66**, 6525–6543.
22 D.-R. Hermann, D. Lilek, C. Daffert, I. Fritz, S. Weinberger, V. Rumpler, B. Herbinger and K. Prohaska, *Analyst*, 2020, **145**, 5242–5251.
23 M. J. Oliveira, R. J. Rubira, L. N. Furini, A. Batagin-Neto and C. J. Constantino, *Appl. Surf. Sci.*, 2020, **517**, 145786.
24 S. Wu, S. Altenried, A. Zogg, F. Zuber, K. Maniura-Weber and Q. Ren, *ACS Omega*, 2018, **3**, 6456–6464.
25 J. Wang, J. Jing, L. Feng, H. Zhu, Z. Hu and X. Ma, *Sustainable Chem. Pharm.*, 2021, **23**, 100500.
26 N. Leopold and B. Lendl, *J. Phys. Chem. B*, 2003, **107**, 5723–5727.
27 P. Lee and D. Meisel, *J. Phys. Chem.*, 1982, **86**, 3391–3395.
28 L. P. de Faria Peixoto, S. D. Pandey, M. B. Barbosa, C. L. Fantini, M. T. da Silva, R. A. Fontes, L. A. Sacorague, R. M. de Carvalho and I. M. F. Lopes, *Spectrochim. Acta, Part A*, 2024, **308**, 123752.
29 *ISO 22412:2017 Particle size analysis–Dynamic light scattering (DLS)*, International Organization for Standardization, 2017.
30 C. A. Lieber and A. Mahadevan-Jansen, *Appl. Spectrosc.*, 2003, **57**, 1363–1367.
31 R. R. Naujok, R. V. Duevel and R. M. Corn, *Langmuir*, 1993, **9**, 1771–1774.
32 G. N. Mathioudakis, A. Soto Beobide, G. Bokias, P. G. Koutsoukos and G. A. Voyiatzis, *J. Raman Spectrosc.*, 2020, **51**, 452–460.
33 S. Kruszewski and M. Cyrankiewicz, *Acta Phys. Pol., A*, 2012, **121**, 68–74.
34 G. Mie, *Ann. Phys.*, 1908, **330**, 377–445.
35 A. Amirjani, F. Firouzi and D. F. Haghshenas, *Plasmonics*, 2020, **15**, 1077–1082.
36 A. Baldi, *Mie_Scattering_and_Absorption_Sphere*, 2022, **https://github.com/andrea-baldi/Mie_Scattering_and_Absorption_Sphere/releases/tag/v1.0.2**.
37 P. B. Johnson and R. W. Christy, *Phys. Rev. B: Solid State*, 1972, **6**, 4370–4379.
38 S. M. Shaban, I. Aiad, F. A. Yassin and A. Mosalam, *J. Surfactants Deterg.*, 2019, **22**, 1445–1460.
39 M. Mahmood, M. Abid, M. F. Nazar, M. N. Zafar, M. A. Raza, M. Ashfaq, A. M. Khan, S. H. Sumrra and M. Zubair, *Mater. Adv.*, 2020, **1**, 2332–2338.
40 G.-N. Xiao and S.-Q. Man, *Chem. Phys. Lett.*, 2007, **447**, 305–309.